

Article

A High-Performance Circularly Polarized and Harmonic Rejection Rectenna for Electromagnetic Energy Harvesting

Zaed S. A. Abdulwali ¹, Ali H. Alqahtani ^{2,*}, Yosef T. Aladadi ¹, Majeed A. S. Alkanhal ¹,
Yahya M. Al-Moliki ¹, Khaled Aljaloud ² and Mohammed Thamer Alresheedi ¹

¹ Department of Electrical Engineering, King Saud University, Riyadh 11421, Saudi Arabia; zabdulwali@ksu.edu.sa (Z.S.A.A.); yaladadi@ksu.edu.sa (Y.T.A.); majeed@ksu.edu.sa (M.A.S.A.); yalmoliki@ksu.edu.sa (Y.M.A.-M.); malresheedi@ksu.edu.sa (M.T.A.)

² Department of Applied Electrical Engineering, Al-Muzahimya Campus, College of Applied Engineering, King Saud University, Riyadh 11421, Saudi Arabia; kaljaloud@ksu.edu.sa

* Correspondence: ahqahtani@ksu.edu.sa

Abstract: This paper presents a novel circularly polarized rectenna designed for efficient electromagnetic energy harvesting at the 2.45 GHz ISM band. A compact antenna structure is designed to achieve high performance in terms of radiation efficiency, axial ratio, directivity, effective area, and harmonic rejection over the entire bandwidth of the ISM frequency band. The optimized rectifier circuit enhances the RF harvested energy efficiency, with an AC-to-DC conversion efficiency ranging from 36% to 70% for low-level input power ranging from -10 dBm to 0 dBm. The stable output of DC power confirms the suitability of this design for various practical applications, including wireless sensor networks, energy harvesting power supplies, medical implants, and environmental monitoring systems. Experimental validation, which includes both the reflection coefficient and radiation patterns of the designed antenna, confirms the accuracy of the simulation. The study found that the proposed energy harvesting system has a high total efficiency ranging from 53% to 63% and is well-suited for low-power energy harvesting (0 dBm) from ambient electromagnetic radiation. The proposed circularly polarized rectenna is a competitive option for efficient electromagnetic energy harvesting, both as a standalone unit and in an array, due to its high performance, feasibility, and versatility in meeting various energy harvesting requirements. This makes it a promising and cost-effective solution for various wireless communication applications, offering great potential for efficient energy harvesting from ambient electromagnetic radiation.

Keywords: RF energy harvesting; circularly polarized antenna; harmonic rejection; stable DC power



Citation: Abdulwali, Z.S.A.; Alqahtani, A.H.; Aladadi, Y.T.; Alkanhal, M.A.S.; Al-Moliki, Y.M.; Aljaloud, K.; Alresheedi, M.T. A High-Performance Circularly Polarized and Harmonic Rejection Rectenna for Electromagnetic Energy Harvesting. *Sensors* **2023**, *23*, 7725. <https://doi.org/10.3390/s23187725>

Academic Editors: Onel Luis Alcaraz López and Katsuya Suto

Received: 17 August 2023
Revised: 31 August 2023
Accepted: 4 September 2023
Published: 7 September 2023



Copyright: © 2023 by the authors. Licensee MDPI, Basel, Switzerland. This article is an open access article distributed under the terms and conditions of the Creative Commons Attribution (CC BY) license (<https://creativecommons.org/licenses/by/4.0/>).

1. Introduction

Electromagnetic (EM) energy harvesting has received a lot of attention for a long time. In the early 1900s, Nikola Tesla experimented with wirelessly transmitting power through microwaves. However, his work was largely left unimplemented, as his experiments were vastly ahead of their time and the technology did not yet exist to make energy harvesting via microwaves feasible [1]. Advances in wireless technologies in the last few decades have made far-field energy harvesting a useful technology that has numerous applications and benefits, such as the Internet of Things (IoT), RF identification (RFID), wireless sensor networks (WSNs), and more [2–5].

Electromagnetic energy harvesting relies heavily on rectifying antennas (rectennas), which can convert RF energy to DC power. The low-pass filter (LPF), diodes, and DC pass capacitor are the main components of the standard rectenna, as shown in the block diagram of Figure 1 [3]. The task of RF power harvesting is performed by converting sent/ambient RF electromagnetic waves into an AC signal through the receiving antenna. This AC signal is then rectified into DC which can be stored in batteries or used directly to drive a specific circuit.



Figure 1. Block diagram of RF energy harvesting system.

The greatest challenge in this system is the nonlinearity of the rectifier circuit, which has some drawbacks. On the one hand, the rectifier conversion efficiency from AC to DC depends on the input power. In other words, the greater the AC input power available at the rectifier, the higher the conversion efficiency that can be achieved, up to a certain point [6]. This issue can be mitigated by improving the performance of the pre-rectifying stages (i.e., the receiving antenna and matching circuit). Therefore, if a proper lossless matching network is used to match the antenna impedance to the rectifier impedance, maximum power transfer is achieved [4]. Consequently, the received antenna is the main part that improves the system's efficiency. The antenna structure should have a high conversion efficiency to convert RF power into AC power [7,8]. Furthermore, the antenna should have a higher capturing efficiency that enables it to capture sufficient RF power to drive the rectifier circuit into the interested region. Increasing capturing efficiency means having a higher radiation efficiency, higher directivity, a lower load mismatching factor, and a lower polarization mismatching factor [9]. In [10], a dual-purpose radial-array rectenna was proposed for RF-energy harvesting IoT sensors, significantly enhancing RF energy capturing from a 360° region. It also enables precise orientation sensing using 5.8 GHz antennas, showcasing its versatility and potential for various applications.

On the other hand, nonlinear rectifying circuits, such as diodes, produce harmonics of the fundamental frequency. The unwanted harmonics impair system performance and result in harmonic interference that reduces the efficiency of the antenna and nearby circuit due to the coupling effect. As a result, a low-pass filter (LPF) is needed to suppress the harmonics to prevent harmonic interference, power re-radiation, and noise with antennas and nearby circuits [11]. However, the LPF will have insertion losses and increase the size and cost of the system. To elevate this effect, filters and microstrip antennas are usually fabricated together on the same substrate to improve cost and efficiency [12]. However, designing an antenna that does not resonate at the second and third resonance frequencies (i.e., also called a filtenna) would be the optimum solution [11]. Additionally, a wide-bandwidth antenna is also preferred, but it comes with decreasing efficiency. Furthermore, the effective bandwidth of the antenna will be limited by the lowest bandwidth of other energy-harvesting circuitry, such as rectifiers, that suffer from decreasing efficiency with increased bandwidth [7,13]. Moreover, improving the mismatching polarization factor makes circularly polarized antennas more preferable to linear polarization for some electromagnetic energy harvesting applications, especially due to the independence of the rotating angle and fading resistance [14].

Therefore, researchers focus on obtaining a competitive design that satisfies the aforementioned aspects or those required by different applications of ambient RF energy harvesting. The antenna used in such systems can be of any type, yet microstrip patch antennas are widely used due to their economical and electromechanical advantages [9,15–18]. However, lower bandwidth, directivity, and efficiency are the main drawbacks of such antennas [19]. Various techniques can be employed to overcome the disadvantages of antenna systems. For instance, using multiple antenna elements in an array can enhance the directivity of the system. However, this comes at the cost of increasing the size of the receiving antenna, which is dependent on the number of elements used. As a result, there is an increasing amount of research being dedicated to the development of compact and highly efficient antenna elements, which can enable the realization of high-performance antenna arrays in a small form factor [14,20–22]. Therefore, an antenna structure that combines harmonic rejection, higher directivity, and efficiency could be a good candidate for low-cost and compact energy harvesting.

In the existing literature, numerous designs have been proposed for electromagnetic energy harvesting applications. However, it is important to note that no single design can be considered perfect or universally suitable for all applications in this field. In [23], compact circularly polarized filtennas at 2.45 GHz are presented, but they have radiation efficiencies of less than 60%. In [24], the authors design a broadband antenna for energy harvesting, but its RF to DC efficiency is less than 55%, and the implementation complexity is high since the filter is printed on another layer. The authors of [25] proposed a highly efficient cross-dipole antenna with a reflector and filter integrated on the same substrate, achieving a high efficiency of 90%. However, the antenna size was very large, approaching the wavelength of the electromagnetic wave.

In [6], two-layer, two-port antennas were used to improve the collected power by obtaining dual linear polarization, but the size and cost of the antenna increased due to the need for two LPF filters, a matching circuit, and a rectifier. In [26], the focus was on minimizing the antenna structures (with maximum dimensions approaching a quarter wavelength) for energy harvesting applications. Although the design achieved a gain of 4.6 dBi and was very compact, it was a linearly polarized antenna with a very narrow bandwidth of 0.55%. In [27], a circularly polarized antenna with a gain of 6 dBi was presented, but the matching and axial ratio (AR) bandwidths were very small at 1.7% and 0.68%, respectively. Additionally, the antenna could not reject harmonics. In [28], a circularly polarized antenna was designed for use in RFID applications with a gain of 6.9 dB, but its bandwidth was limited to 1.5% at 2.45 GHz.

Metamaterial-based energy harvesting structures have also garnered significant attention from researchers due to their unique properties. The ability to engineer a metasurface and metamaterial surface with negative permeability and permittivity has opened up novel applications in various frequency bands, including energy harvesting [29], perfect lensing [30], and perfect absorption [31]. For instance, the metamaterial's integration in the antenna design in [32] leads to a significant enhancement in the antenna's gain across all frequency bands. This notable improvement solidifies the antenna as a promising solution for high-performance wireless communication systems. Moreover, a compact metamaterial-inspired antenna (MIA) enables efficient WiFi energy harvesting without complex networks, producing a rectified DC voltage for powering distributed microsystems [33]. In a related study [34], a dual-band metasurface simplifies design and facilitates high-efficiency electromagnetic energy harvesting at Wi-Fi frequencies, making it suitable for applications such as wireless power transfer. Additionally, an efficient miniaturized metasurface achieves over 78% conversion efficiency at 5.54 GHz, making it ideal for compact wireless sensor networks with wide angles [35]. However, a significant limitation of metamaterials is their narrow bandwidth of operation due to the resonance frequencies of their structures. This bandwidth limitation, coupled with the cost of fabrication, presents a challenge for the practical implementation of metamaterial-based energy harvesting structures. Nonetheless, ongoing research in this area holds great promise for the development of efficient and cost-effective energy harvesting solutions for a wide range of applications.

This paper presents a highly effective area rectenna for the 2.45 GHz ISM band, achieving compactness, circular polarization, high efficiency, harmonic rejection, sufficient improved bandwidth covering the ISM band, and high gain compared to traditional patch antennas. By effectively combining these features in a balanced tradeoff, the design enhances efficiency and expands the potential applications for energy harvesting. The antenna design structure has a bandwidth ratio of 4.08%, a directivity of 7.2 dBi, and a radiation efficiency of 92.5%. Moreover, the total size of the antenna is around 0.5×0.5 wavelength. The antenna can reject the second and third harmonics, which means it can be used without an LPF. The structure is one port and one layer, making it a simple and low-cost design. An optimized rectifier is also presented to evaluate the total rectenna performance and meet the antenna requirements.

2. Rectenna Design

To build a rectenna system, the most important parameters to evaluate the system should be considered. One of these parameters is the received power by the antenna used in this system, which is directly related to the receiving antenna's effective area as [9]

$$P_r = A_{eff} W_{inc} \quad (1)$$

where A_{eff} is the antenna effective area that can be found by Equation (2), and W_{inc} is the incident power density of the plane wave that can also be given by Equation (3).

$$A_{eff} = \tau \eta_{rad} \frac{\lambda^2 D}{4\pi} PLF \quad (2)$$

$$W_{inc} = \frac{|E_i|^2}{2\eta_0} \quad (3)$$

where τ is the matching transmission coefficient of the loaded antenna, which can be given by Equation (4), η_{rad} is the radiation efficiency of the antenna, λ is the wavelength of the incident wave, D is the antenna directivity, PLF is the polarization mismatching loss factor that is given by Equation (5), E_i is the incident electric field intensity, and η_0 is the surrounding medium's characteristic impedance, which is assumed to be air in this research, so $\eta_0 = 120\pi \Omega$.

$$\tau = \frac{4R_A R_L}{|Z_A + Z_L|^2} \quad (4)$$

$$PLF = |\mathbf{a}_i \cdot \mathbf{a}_r|^2, \quad (5)$$

where R_A and Z_A are the receiving antenna input resistance and impedance, respectively; R_L and Z_L are the antenna load resistance and impedance, respectively; \mathbf{a}_i and \mathbf{a}_r are the incident field's instantaneous direction vector and the antenna polarization direction vector, respectively. It must be emphasized that (W_{inc} times $\lambda^2 D / (4\pi)$) is the maximum effective area used to find P_r when there is no mismatching loss (i.e., $\tau = 1$) or polarization mismatching loss (i.e., $PLF = 1$).

2.1. Antenna Geometry

The structure of a slotted circular patch antenna and its main important parameters are shown in Figure 2. The proposed antenna is a single-layer antenna consisting of a slotted circular patch on the front side, which is etched on a 60 mm × 60 mm Roger RT/duroid 5880 dielectric, a fully grounded reflector on the backside, a centered short via connecting the front and back sides, and coaxial probe feeding. The antenna shows the advantages of small size, high efficiency, directivity, and good matching in the 2.45 ISM band with circular polarization. In addition, it has harmonic rejection properties at the second and third harmonics. Thus, it is more suitable for power transfer and energy harvesting applications. This was achieved by minimizing the loss (i.e., increasing the radiation efficiency) and minimizing the rectenna size by self-suppressing the second and third harmonics.

Coaxial probe feeding was chosen because it has low transmission line loss and minimizes the area, thereby reducing the aforementioned problems. The feed position is chosen to achieve right-hand circular polarization.

The antenna is etched on a 60 mm × 60 mm (i.e., $\sim 0.5 \lambda \times 0.5 \lambda$) Roger RT/duroid 5880 substrate with a dielectric constant ($\epsilon_r = 2.2$) and electric tangent loss ($\tan(\delta) = 0.0009$), which are more suitable for enhancing the radiation efficiency. Although a low dielectric constant is not good for radiation characteristics, especially with a thin substrate [16], the proposed antenna has demonstrated good performance, as presented in the next section. The slotted edge is useful for obtaining this advantage since it causes the input impedance of the antenna to be constructively matched with the port impedance.

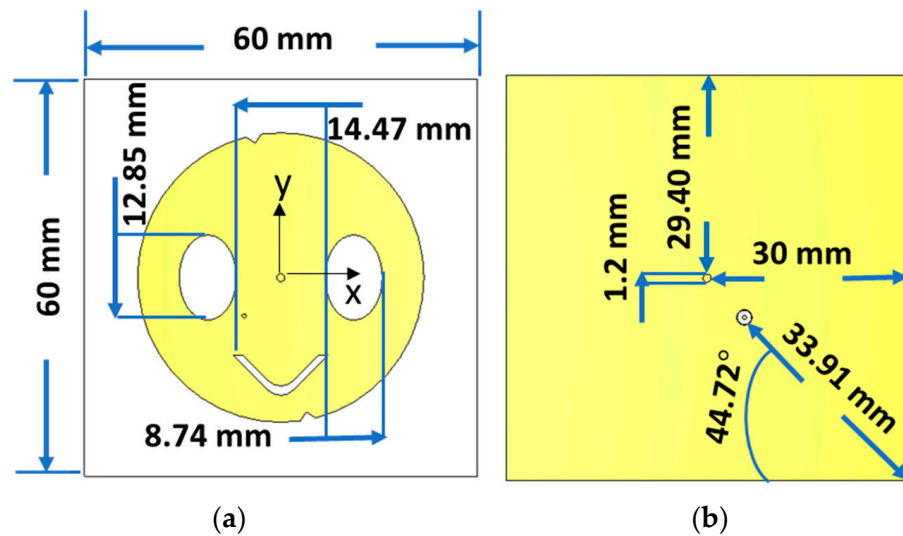


Figure 2. Structure of the proposed antenna, (a) the front side of the antenna, (b) the backside of the antenna.

2.2. Rectifier Design

To build a full rectenna system, a rectification circuit was designed based on the antenna's results. The rectifier circuit schematic built into ADS is shown in Figure 3. The goal was to maximize the DC output power at $1\text{ k}\Omega$, $P_{in} = -10\text{ to }10\text{ dBm}$, and $f = 2.37 - 253\text{ GHz}$.

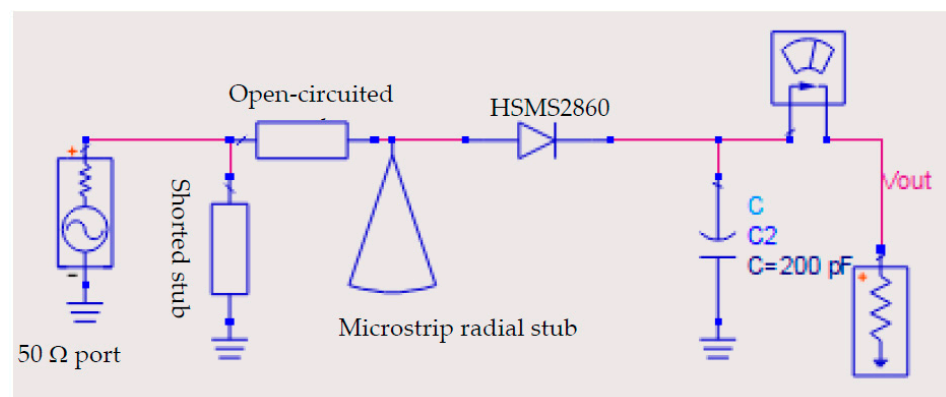


Figure 3. The rectifier circuit schematic with impedance matching circuit.

The design of the rectifier circuit was based on optimizing the microstrip transmission line (impedance matching circuit) with different lengths and widths to achieve the desired goal. To ensure proper impedance matching, a Roger RT5880 substrate with a dielectric constant ($\epsilon_r = 2.2$) and electric tangent loss ($\tan(\delta) = 0.0009$) was used.

To analyze the rectifier in the proposed rectenna system, the Harmonic Balance (HB) simulator was used due to the presence of the nonlinear Schottky diode (HSMS2860). HSMS2860 belongs to the HSMS-286x family of DC-biased detector diodes, which have been designed and optimized for use from 915 MHz to 5.8 GHz. The HSMS-286x family is ideal for RF/ID and RF Tag applications as well as large signal detection, modulation, RF to DC conversion, or voltage doubling. The electrical specification and spice parameter elements of this circuit are defined by the datasheet of the HSMS286x series in [36]. The circuit contains a series of transmission lines, a shorted stub, an open-circuited stub, and a microstrip radial stub between the $50\ \Omega$ port and the HSMS2860 diode.

To achieve optimal performance, a series HSMS 2860 Schottky diode was selected for its low turn-on voltage and fast switching speed at a frequency of operation of 2.45 GHz.

Additionally, a shunt capacitor of 200 pF was chosen to appear as a short circuit for GHz frequencies and an open circuit for the rectified DC power.

Table 1 shows the optimized parameters of the impedance matching circuits, which were critical in achieving high AC-to-DC conversion efficiency ranging from 36% to 70% for low input power levels.

Table 1. Simulation results.

Shorted Stub L_1/W_1	Open-Circuited Stub L_2/W_2	Microstrip Radial Stub $L_3/W_3/\theta_3$
7.71/8.67	4/0.1	8.73/0.707/78°

3. Simulation Results

The antenna port is excited by a Gaussian pulse with a 50 Ω probe feeding, propagating from the back of the antenna towards a positive z-axis direction, as depicted in Figure 2. To solve the electromagnetic problem with open boundaries (far-field problem), the finite integration technique (FIT) solver in Computer Simulation Technology (CST) is utilized. Furthermore, practical measurements are employed to validate the designed antenna and ensure its performance in real-world scenarios. In parallel, the performance evaluation of the proposed rectifier is carried out using the Harmonic Balance (HB) technique within the ADS full-wave simulator. This approach allows for a comprehensive analysis of the rectifier's behavior and efficiency.

3.1. Antenna Reflection Coefficient and Input Impedance

The reflection coefficient (S_{11}) of a 50 Ω port as well as the input impedance of the antenna are shown in Figure 4. The antenna has a bandwidth of around 100 MHz with $S_{11} < -10$ dB, which covers the whole ISM bandwidth.

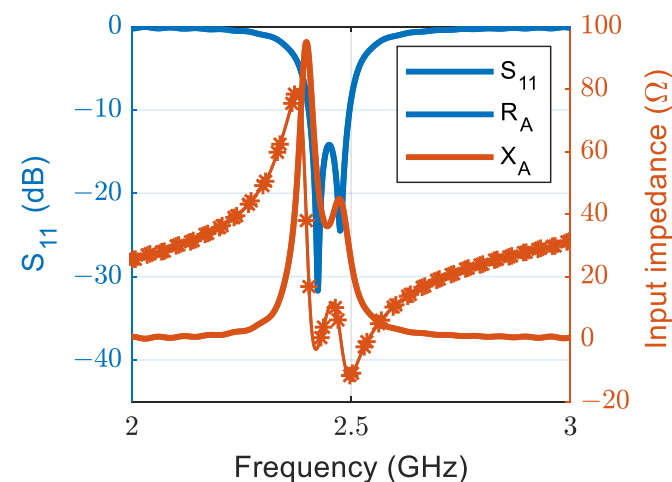


Figure 4. Return loss and input impedance of the final-designed antenna.

The antenna design process is arranged into five stages. The first stage started by selecting the structure that would minimize the size and achieve good performance at the required bandwidth of 2.45 GHz in the ISM band. Thus, a probe-fed circular-patch microstrip antenna with Roger RT/duroid 5880 low permittivity and loss substrate material is first chosen based on recommendations in [17]. Then, using the design formula Equation (6) in [9], the radius of the circular patch, r , is calculated at the center resonance frequency, 2.45 GHz, using Roger RT/duroid 5880 material of a 2.2 permittivity (ϵ_r) and 1.6 mm thickness (h). The radius calculation result of 23.13 mm is used to simulate the circular

patch antenna using the full-wave simulator, where the feeding position and ground size are also chosen according to the recommendations of [9,17].

$$r = \frac{F}{\left\{1 + \frac{2h}{\pi\epsilon_r F} \left[\ln\left(\frac{\pi F}{2h}\right) + 1.7726\right]\right\}^{1/2}}, \quad F = \frac{8.791 \times 10^9}{f_r \sqrt{\epsilon_r}} \quad (6)$$

Figure 5a shows the circular structure with the S_{11} of the five design process stages. The first stage (stage #1) is to adjust the antenna size for the targeted ISM band without any perturbations. In this stage, the antenna has a resonating mode of around 2.45 GHz and also resonates around the second and third harmonics. Furthermore, the radiation in this case is linear, and the antenna bandwidth is only 42 MHz. Therefore, the following design process stages are to solve these challenges by allowing suitable current perturbations to change the linear polarization to circular, increase the bandwidth, and reject the second and third harmonics. To have circular polarization, two orthogonal modes are generated in the second stage by loading the antenna with two optimum symmetric oval slots, as shown in Figure 2, and locating the feeding at 45° from the slot axis. The symmetric slots also improve the bandwidth and help minimize the radius of the circular patch from 23.13 mm to 21.86 mm. The size and position of these slots are adjusted and optimized to achieve the desired bandwidth and polarization axial ratio. The achieved bandwidth is 100 MHz, as shown in Figure 5a (see stage #2 line). The third stage (stage #3) aims to reject the harmonic where the patch antenna is loaded with a V-slot on its center bottom side to reject the second and third harmonics. The symmetric position with optimized dimensions of the V-slot improves the harmonic rejection property. To finely adjust the axial ratio and improve the matching, two triangular slits were introduced in the fourth stage (stage #4). In the last stage (stage #5), a centered via is used to further suppress the second and third harmonic frequencies at the second and third resonances. Therefore, this structure works as a filtenna since it works as a stop-band filter for harmonics, as shown in Figure 5b. Harmonics can cause rectenna performance degradation as well as nearby circuitry degradation, as explained in the introduction. Accordingly, the antenna is suitable for energy harvesting applications. The most important performance parameters that affect the effective area of the antenna are discussed in the next section.

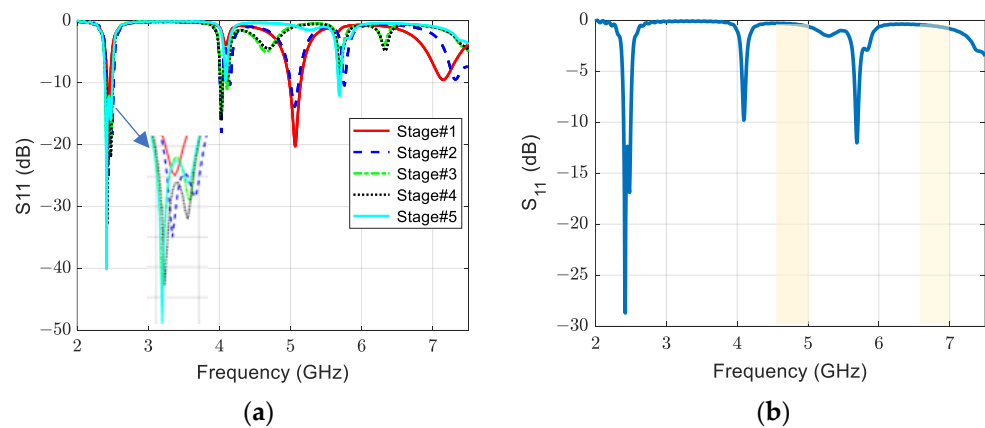


Figure 5. The reflection coefficient of (a) five design process stages and (b) final optimized stage.

Figure 6 shows the current distribution of the proposed right-hand circularly polarized antenna at 2.45 GHz, which varies at different phases, indicating the counterclockwise movement of the surface current distribution at the edges. At all phases, the current distribution exhibits maximum amplitude at the symmetric oval slots, V-slot, and edges.

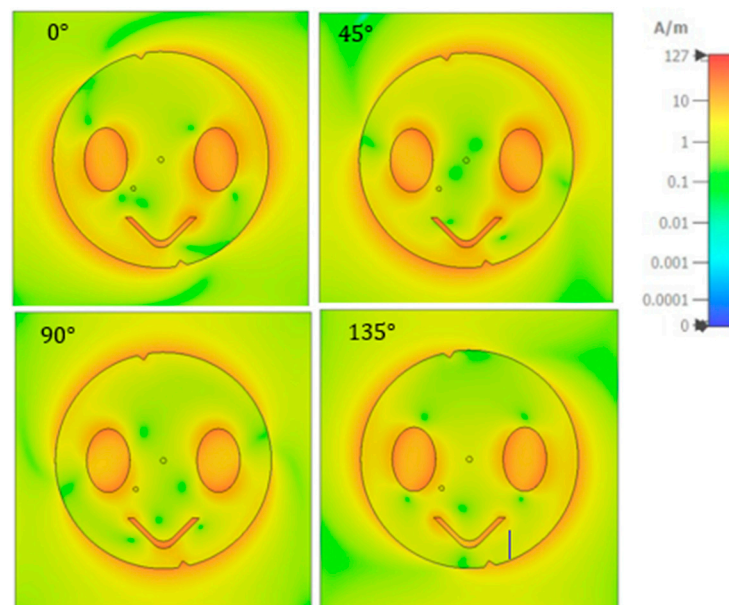


Figure 6. Current distribution of the proposed antenna at 2.45 GHz and different phases.

3.2. Antenna Radiation Efficiency and Axia Ratio

The proposed antenna structure exhibits a radiation efficiency that varies between 80% and 91% over the frequency bandwidth of the ISM band, as shown in Figure 7. This is a significant achievement, as high radiation efficiency is critical for converting RF power into AC power for energy harvesting applications.

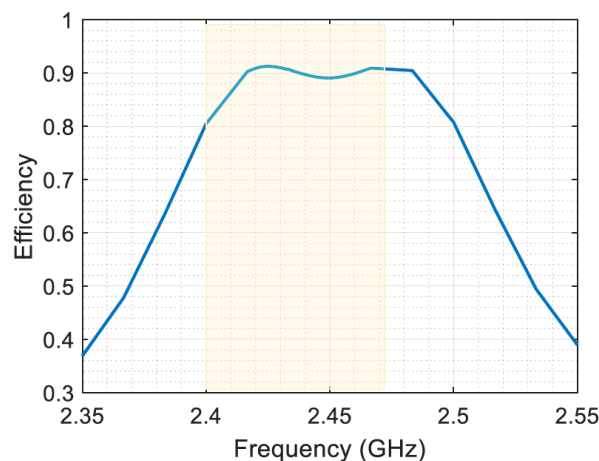


Figure 7. Antenna radiation efficiency.

Figure 8 shows the axial ratio performance of a circularly polarized antenna over a specific frequency range from 2.35 GHz to 2.55 GHz. The axial ratio, which is a measure of the polarization purity of an antenna, is plotted as a function of frequency, with the relevant frequency range highlighted for clarity. The results show that the proposed antenna is circularly polarized around the 2.45 GHz frequencies. The antenna exhibits outstanding circular polarization purity with an axial ratio consistently less than 3 dB. The fact that the axial ratio remains very small over the entire frequency range of interest is a testament to the antenna's exceptional performance and its ability to maintain the desired polarization state with minimal distortion. Consequently, the amount of captured power will be increased to match the circular polarization and be half the amount for linear polarization ambient EM waves.

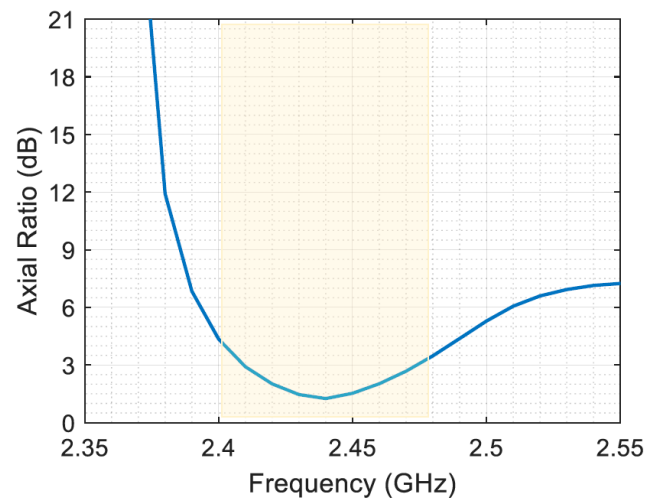


Figure 8. The axial ratio performance of a circularly polarized antenna.

3.3. Antenna Directivity and Effective Area

The co-polarized directivity pattern of the proposed antenna at the studied frequency is shown in Figure 9. The maximum directivity is around 7.2 dBi in the main lobe of the center operating frequency, 2.45 GHz. The radiation pattern is unidirectional and symmetric in both the azimuth and elevation planes, with no significant side or back lobes. The plot of directivity with frequency variation in the same main lobe direction is shown in Figure 10a. The directivity of the antenna indicates its ability to concentrate radiation in a specific direction. However, directivity alone is not sufficient for a complete understanding of the antenna's performance. To assess its effectiveness, it is important to consider the gain and realized gain as well. Gain refers to the ratio of the power radiated by the antenna in a specific direction to the power that an ideal isotropic antenna would radiate, assuming the same input power. It quantifies the antenna's ability to efficiently radiate energy in a specific direction.

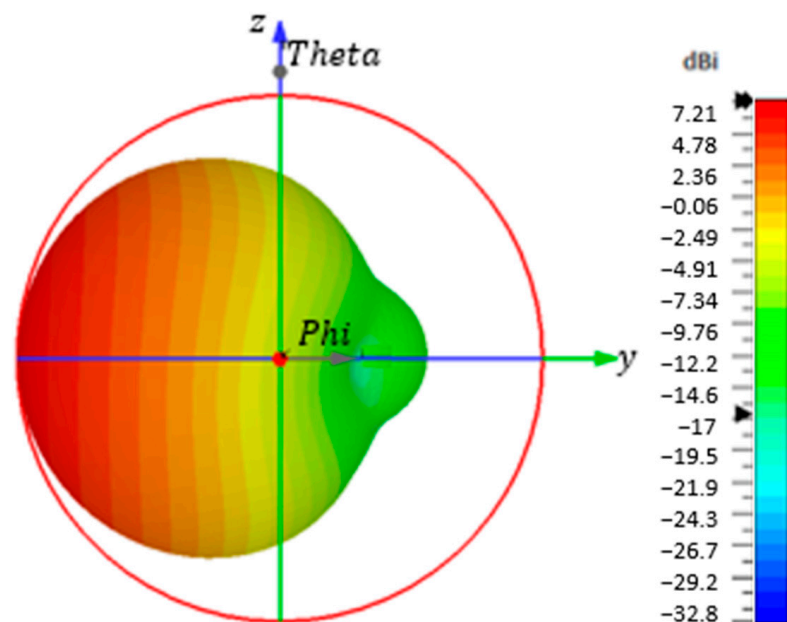


Figure 9. The antenna directivity pattern at 2.45 GHz.

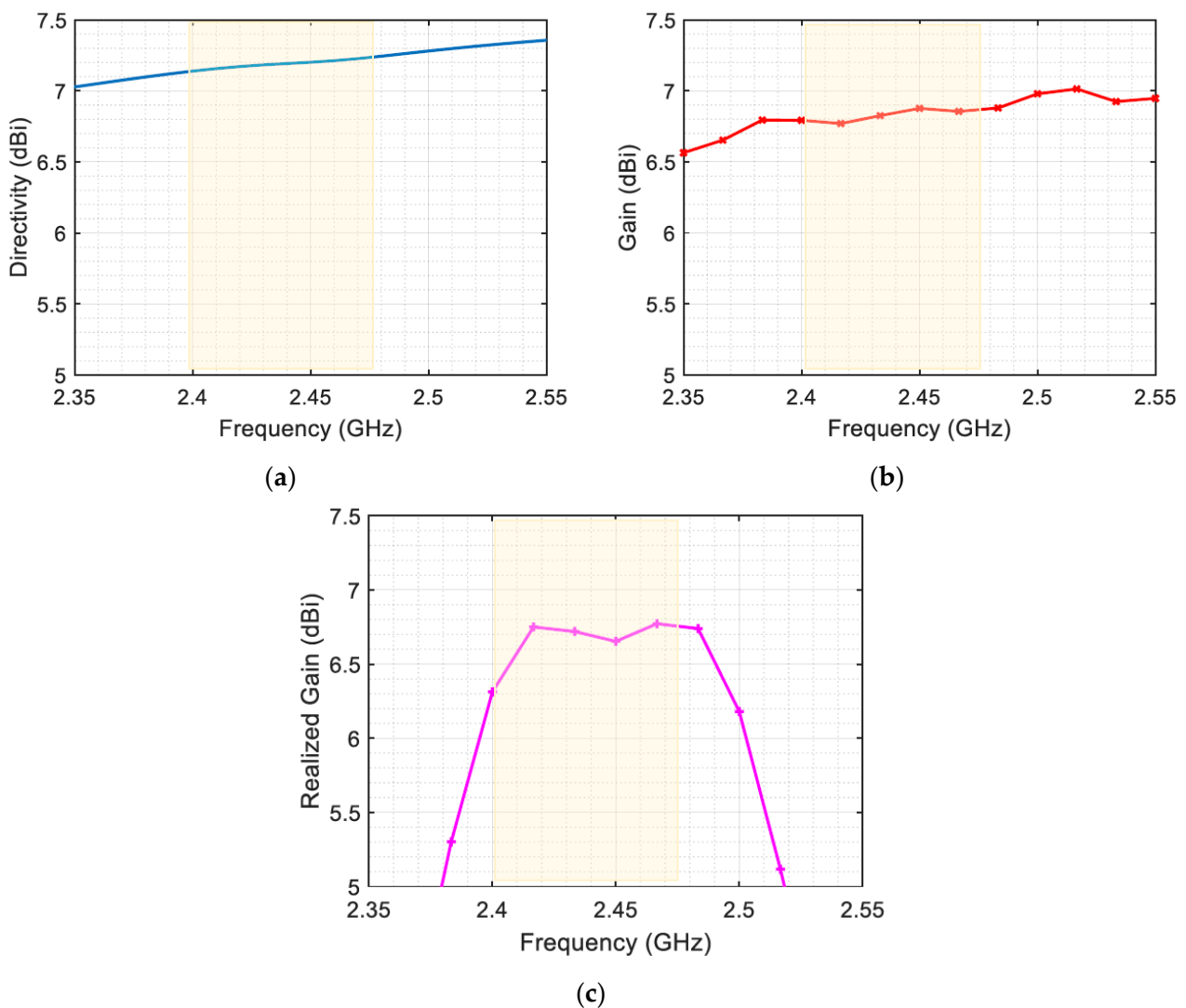


Figure 10. (a) Antenna directivity, (b) gain, and (c) realized gain vs. frequency.

On the other hand, realized gain takes into account various factors such as losses, impedance matching, and efficiency. It provides a more realistic measure of the antenna's performance in practical applications. Figure 10b,c present the antenna's gain and realized gain, respectively.

In the context of energy harvesting, the effective area is a critical parameter, as it determines how much energy can be harvested from the ambient electromagnetic waves. Once the incident field is co-polarized with the antenna structure (i.e., $PLF \approx 1$) and the connected load circuit is conjugate-matched ($\tau \approx 1$), the maximum absorbed power is obtained. According to Equation (2), the effective area of the proposed antenna varies between 36 cm^2 and 55 cm^2 over the frequency range of 2.4 to 2.5 GHz.

A performance comparison between various published works and the proposed antenna is listed in Table 2. Among the listed designs, the proposed antenna exhibits a better trade-off between minimization, bandwidth, efficiency, and self-filtering for harmonic rejection (i.e., performing the LPF task). This makes it sufficient to drive the rectifier circuit for the targeted application with a low level of incident EM power.

Table 2. Comparison of antenna performance with the literature.

Ref.	Dimensions (λ)	Radiation Efficiency	Relative Bandwidth	Directivity	LPF Feature
[13]	$0.49 \times 0.49 \times 0.0136$	45%	5.3%	6.7 dBi	No
[24]	$0.49 \times 0.49 \times 0.0136$	50%	5.3%	6.9 dBi	Yes
[27]	$0.46 \times 0.46 \times 0.03$	89%	1.5%	6.98 dBi	-
[26]	$0.474 \times 0.474 \times 0.0158$	86%	1.7%	6.8 dBi	-
This work	$0.49 \times 0.49 \times 0.0136$	92%	4.08%	7.2 dBi	Yes

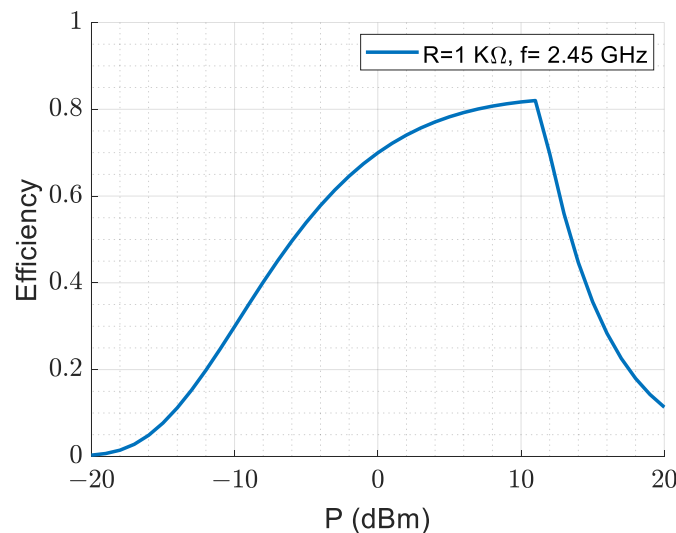
3.4. AC–DC Efficiency

The efficiency of converting the received AC power to DC power is critical for energy harvesting applications. The AC-to-DC power conversion efficiency is calculated using Equation (7).

$$\eta_{Ac-DC} = \frac{V_o \times I_o}{P_{in}} \quad (7)$$

where P_{in} is the total time-average power coupled to the 50Ω input port of the impedance matching network, and V_o and I_o are the output voltage and current on the load of the DC filter.

Figure 11 illustrates the AC-to-DC conversion efficiency at 2.45 GHz with a $1 \text{ K}\Omega$ rectifier resistive load. The junction resistance in the equivalent circuit model of an HSMS 2860 Schottky diode [36] is dependent on the externally applied bias current, which makes AC-to-DC radiation conversion efficiency depend on the input power levels. The results show that for low input power levels ranging from -10 dBm to 0 dBm , the efficiency gradually increases from around 36% to 70%. The maximum DC power inversion occurs at an input AC power of 10 dBm . However, it is important to note that the performance of conversion efficiency deteriorates for higher input power levels ($>11 \text{ dBm}$).

**Figure 11.** AC-to-DC radiation conversion efficiency.

For practical wireless communication applications, the received input power levels are typically between -10 dBm and 0 dBm (an interesting region). Therefore, the proposed antenna structure with a rectifier circuit with AC-to-DC radiation conversion efficiency ranging from 36% to 70% for low input power levels is suitable for energy harvesting from wireless communication signals. The results demonstrate the advantages of the proposed rectenna for efficient energy harvesting from ambient electromagnetic radiation, which could be useful in various applications.

The overall efficiency of the energy harvesting system is affected by various factors, including the resistive load of the rectifier. Figure 12 shows the effect of changing the resistive load of the rectifier on the output DC power. Electromagnetic energy harvesting is utilized in various applications, including wireless sensor networks, RFID systems, energy harvesting power supplies, medical implants, and environmental monitoring systems. The input impedance of these applications varies, with wireless sensor networks typically ranging from 1 k Ω to 10 k Ω , RFID systems ranging from 50 Ω to 100 Ω , and others typically ranging from 1 k Ω to 100 k Ω [37]. The results of this work indicate that the DC power is stable in the range of 1 K Ω to 4 K Ω resistive load rectifiers for practical input AC power levels (−10 dB to 0 dB), which makes it a suitable candidate to support wireless sensor networks, energy harvesting power supplies, medical implants, and environmental monitoring systems.

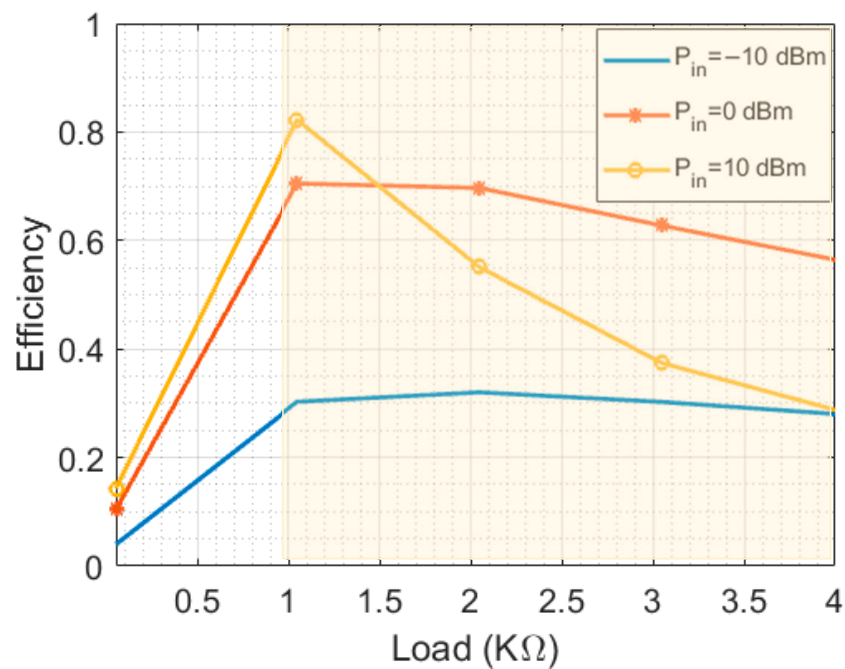


Figure 12. AC-to-DC radiation conversion efficiency at 2.45 GHz.

In addition to the resistive load, the energy harvesting performance also varies with the input AC power level and operating frequency. Figure 13 shows the AC-to-DC conversion efficiency for frequencies in the ISM band at three different input AC power levels. The results indicate that the efficiency is within the range of 20% to 75% for the targeted bandwidth and different input power levels ranging from −10 dBm to 0 dBm.

Figure 14 presents the total efficiency of the energy harvesting system, which includes both AC-to-AC and AC-to-DC conversion efficiencies, plotted against frequency for the 0 dBm input power level and 1 K Ω resistive load. The results demonstrate that the proposed energy harvesting system offers a high total efficiency, ranging from 53% to 63%.

The high total efficiency of the energy harvesting system has important implications for various applications where low-power energy harvesting is essential. The results highlight the potential of the proposed antenna structure and energy harvesting system to provide a cost-effective and efficient energy harvesting solution for various wireless communication applications.

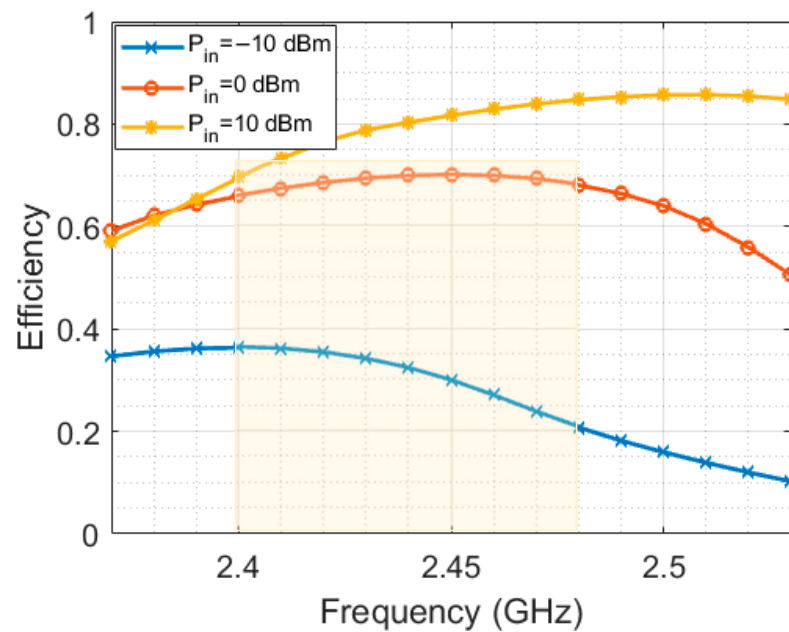


Figure 13. AC-to-DC radiation conversion efficiency at 1 K Ω resistive load.

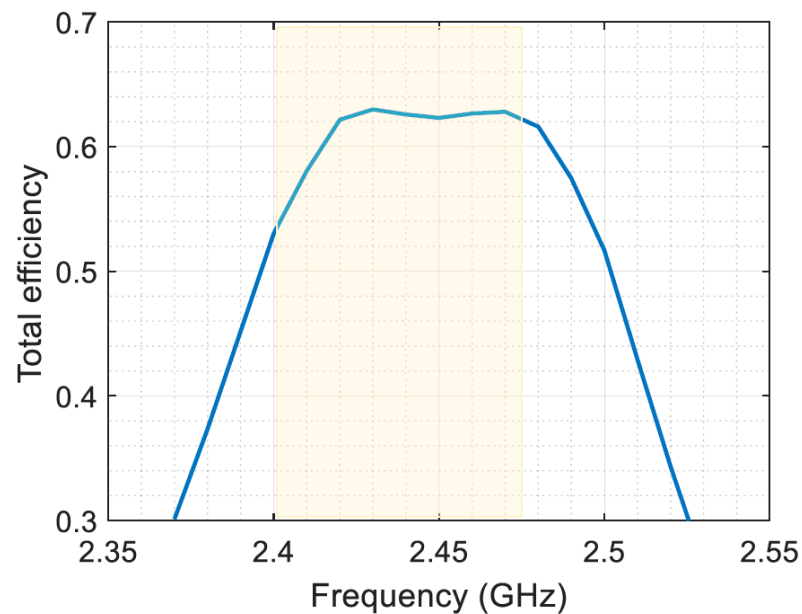


Figure 14. Total efficiency at 1 K Ω resistive load and 0 dBm input power.

3.5. Experimental Validation

This section provides experimental validation of the antenna simulation results. A comparison is performed by analyzing the reflection coefficients and radiation patterns of both the simulated and measured data.

The fabricated antenna and vector network analyzer system are shown in Figure 15. Figure 16 presents a comparison between the measured and simulated S_{11} values of the designed antenna, which indicates good agreement between the simulation and measurement results. This agreement confirms that the designed antenna is highly accurate and reliable.

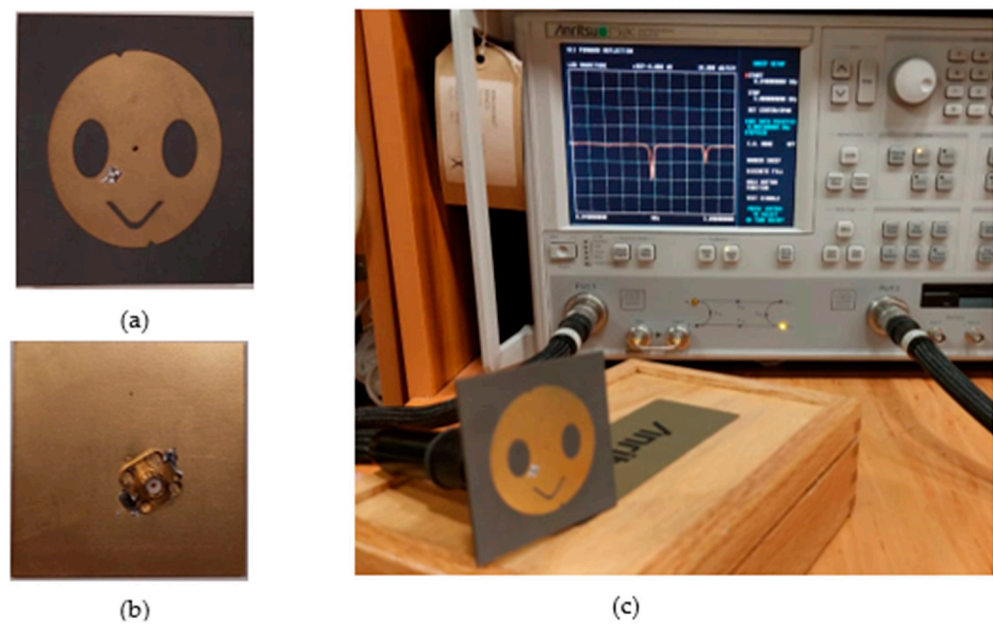


Figure 15. The fabricated antenna with vector network analyzer system. (a) The front side of the antenna, (b) the backside of the antenna, and (c) the vector network analyzer measurement system with the proposed antenna.

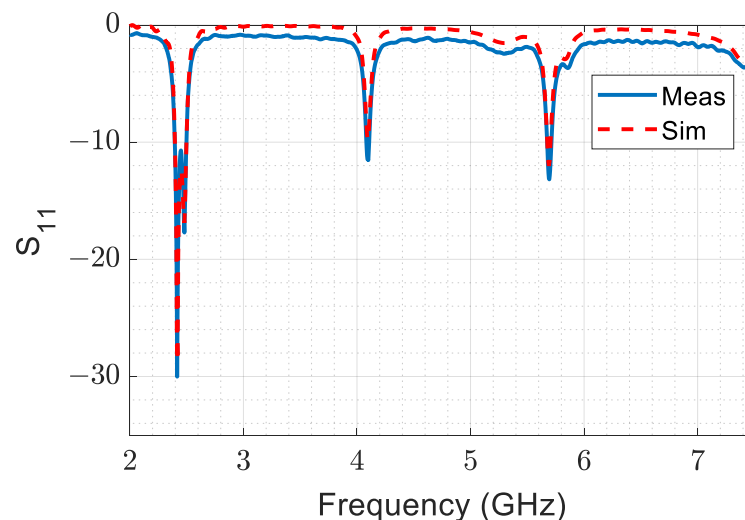


Figure 16. The measured and simulated reflection coefficients, S_{11} .

Figure 17 shows the Geozondas [38] time-domain antenna measurement setup used for measuring the radiation pattern of the designed antenna in the time domain. This setup consists of a pulsed signal generator, a digital sampling converter, a transmitting antenna, a receiving antenna, and an oscilloscope. The pulsed signal generator sends a short pulse to the transmitting antenna, which then radiates the pulse into space. The receiving antenna captures the signal, which is then analyzed by the oscilloscope to determine the receiving antenna's radiation pattern. Figure 18a,b illustrates the measured and simulated polar radiation patterns of the designed antenna in the azimuth and elevation planes, respectively. The agreement between the simulation and measurement results demonstrates the accuracy and reliability of the designed antenna. The close match between the two sets of data in both the reflection coefficients and radiation patterns provides strong evidence to support the validity of the simulation approach and its ability to predict the behavior of the whole rectenna (antenna and rectifier) system.

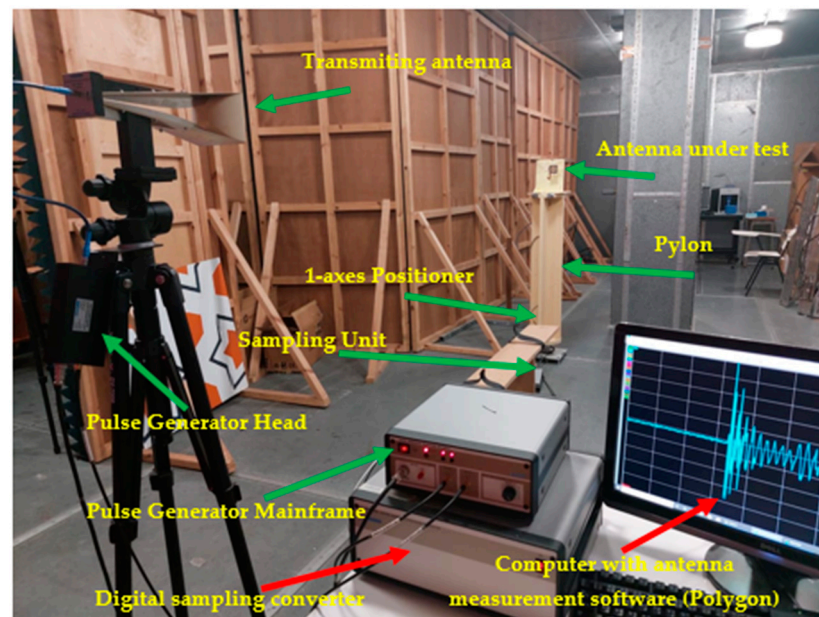


Figure 17. Geozondas time-domain antenna measurement setup.

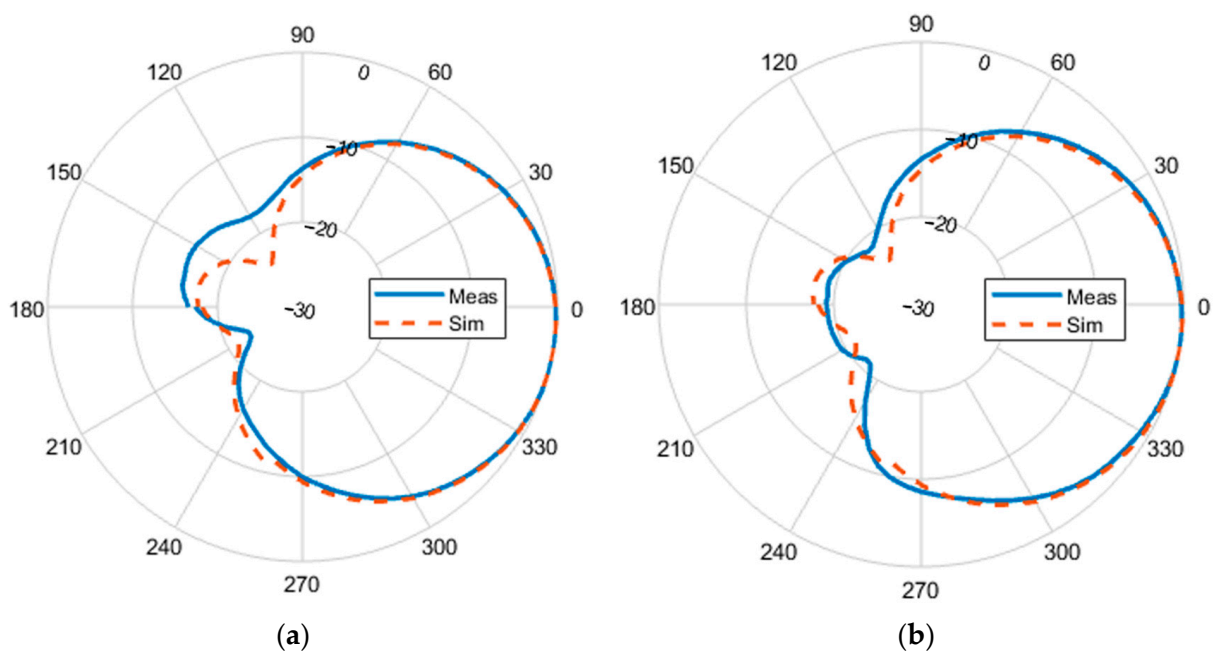


Figure 18. Normalized circularly polarized radiation patterns at 2.45 GHz: (a) azimuth and (b) elevation plane.

The gain is measured by calculating the performance of the proposed antenna in comparison to a reference antenna with a known gain. The two antennas are connected alternately to the same transmitter, and the received power is measured for each antenna. Both used antennas, the reference and the transmitter, are double-ridged horn antennas with lens GZ0126 DRH (see Figure 17). The gain of the proposed antenna is then determined by comparing the power levels. The measured gain of the proposed antenna is depicted in Figure 19, demonstrating an accepted agreement with the simulated gain.

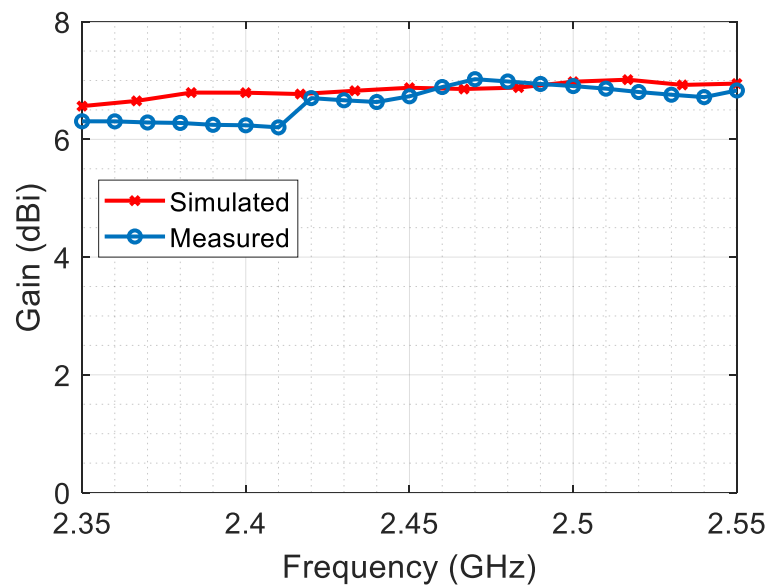


Figure 19. The measured gain compared to the simulation gain.

4. Conclusions

This paper presents a circularly polarized rectenna designed for high-performance electromagnetic energy harvesting in the 2.45 GHz ISM frequency band. The proposed antenna structure achieves a radiation efficiency ranging from 80% to 91%, an effective area between 36 cm² and 55 cm², an axial ratio consistently less than 3 dB, and harmonic rejection over the bandwidth of the ISM band. Furthermore, it achieves a directivity of 7.2 dBi in the main lobe direction with negligible side/back lobes at the center frequency. The optimized rectifier enhances the RF harvested energy efficiency, with an AC-to-DC conversion efficiency ranging from 36% to 70% for input power levels ranging from −10 dBm to 0 dBm. The proposed design is feasible, versatile, and a competitive option for electromagnetic energy harvesting applications as a single element or in an array to meet various energy harvesting requirements. The stable output DC power in the range of 1 K Ω to 4 K Ω resistive load rectifiers for practical input AC power levels (−10 dB to 0 dB) confirms the suitability of this design for various applications, including wireless sensor networks, energy harvesting power supplies, medical implants, and environmental monitoring systems.

Additionally, the study finds that the proposed energy harvesting system has a high total efficiency that ranges from 53% to 63% at 0 dBm ambient electromagnetic power. Therefore, it is well suited for low-power energy harvesting, which has significant implications for various wireless communication applications.

The manufactured novel circularly polarized antenna was tested for its radiation pattern and S_{11} characteristics, with simulation and measurement results exhibiting remarkable agreement.

Author Contributions: Conceptualization, Z.S.A.A., Y.T.A. and M.A.S.A.; software, Z.S.A.A. and Y.T.A.; validation, Z.S.A.A., Y.T.A., Y.M.A.-M. and M.A.S.A.; formal analysis, Z.S.A.A., Y.T.A., Y.M.A.-M. and K.A.; investigation, Z.S.A.A. and Y.T.A.; resources, A.H.A. and M.T.A.; data curation, Z.S.A.A. and Y.T.A.; writing—original draft preparation, Z.S.A.A., Y.T.A. and Y.M.A.-M.; writing—review and editing, Z.S.A.A., A.H.A., Y.T.A., Y.M.A.-M. and M.A.S.A.; visualization, Z.S.A.A., A.H.A. and K.A.; supervision, A.H.A. and M.A.S.A.; project administration, A.H.A., K.A. and M.T.A.; funding acquisition, A.H.A., K.A. and M.T.A. All authors have read and agreed to the published version of the manuscript.

Funding: This research was funded by the Deputyship for Research and Innovation, the “Ministry of Education” in Saudi Arabia, grant number IFKSUDR_E169.

Institutional Review Board Statement: Not applicable.

Informed Consent Statement: Not applicable.

Data Availability Statement: Data sharing not applicable.

Acknowledgments: The authors extend their appreciation to the Deputyship for Research and Innovation, the “Ministry of Education” in Saudi Arabia, for funding this research work through the project number (IFKSUDR_E169).

Conflicts of Interest: The authors declare no conflict of interest.

References

1. Brown, W.C. The History of Power Transmission by Radio Waves. *IEEE Trans. Microw. Theory Tech.* **1984**, *32*, 1230–1242. [[CrossRef](#)]
2. Schlesak, J.J.; Alden, A.; Ohno, T. Microwave powered high altitude platform. *IEEE MTT-S Int. Microw. Symp. Dig.* **1988**, *1*, 283–286.
3. Srinivasu, G.; Sharma, V.K.; Nella, A. A Survey on Conceptualization of RF Energy Harvesting. *J. Appl. Anal. Comput.* **2019**, *6*, 791–800.
4. Valenta, C.R.; Durgin, G.D. Harvesting wireless power: Survey of energy-harvester conversion efficiency in far-field, wireless power transfer systems. *IEEE Microw. Mag.* **2014**, *15*, 108–120.
5. Zhang, Z.; Pang, H.; Georgiadis, A.; Cecati, C. Wireless Power Transfer—An Overview. *IEEE Trans. Ind. Inform.* **2019**, *66*, 1044–1058. [[CrossRef](#)]
6. Sun, H.; Geyi, W. A New Rectenna with All-Polarization-Receiving Capability for Wireless Power Transmission. *IEEE Antennas Wirel. Propag. Lett.* **2016**, *15*, 814–817. [[CrossRef](#)]
7. Wagih, M.; Weddell, A.S.; Beeby, S. Rectennas for radio-frequency energy harvesting and wireless power transfer: A review of antenna design [Antenna Applications Corner]. *IEEE Antennas Propag. Mag.* **2020**, *62*, 95–107. [[CrossRef](#)]
8. Abdulhasan, R.A.; Mumin, A.O.; Jawhar, Y.A.; Ahmed, M.S.; Alias, R.; Ramli, K.N.; Homam, M.J.; Audah, L.H.M. Antenna Performance Improvement Techniques for Energy Harvesting: A Review Study. *Artic. Int. J. Adv. Comput. Sci. Appl.* **2017**, *8*, 97–102.
9. Balanis, C.A. *Antenna Theory: Analysis and Design*, 4th ed.; John Wiley & Sons: Hoboken, NJ, USA, 2016.
10. Kumar, M.; Kumar, S.; Sharma, A. Dual-purpose planar radial-array of rectenna sensors for orientation estimation and RF-energy harvesting at IoT nodes. *IEEE Microw. Wirel. Compon. Lett.* **2022**, *32*, 245–248. [[CrossRef](#)]
11. Divakaran, S.K.; Das Krishna, D.; Nasimuddin. RF energy harvesting systems: An overview and design issues. *Int. J. RF Microw. Comput.-Aided Eng.* **2019**, *29*, e21633. [[CrossRef](#)]
12. Suh, Y.H.; Chang, K. A high-efficiency dual-frequency rectenna for 2.45- and 5.8-GHz wireless power transmission. *IEEE Trans. Microw. Theory Tech.* **2002**, *50*, 1784–1789. [[CrossRef](#)]
13. Lin, Y.L.; Zhang, X.Y.; Du, Z.X.; Lin, Q.W. High-efficiency microwave rectifier with extended operating bandwidth. *IEEE Trans. Circuits Syst. II Express Briefs* **2018**, *65*, 819–823. [[CrossRef](#)]
14. Yo, T.C.; Lee, C.M.; Hsu, C.M.; Luo, C.H. Compact circularly polarized rectenna with unbalanced circular slots. *IEEE Trans. Antennas Propag.* **2008**, *56*, 882–886. [[CrossRef](#)]
15. Bakkali, A.; Pegleri-Sebastia, J.; Sogorb, T.; Llario, V.; Bou-Escriva, A. A Dual-Band Antenna for RF Energy Harvesting Systems in Wireless Sensor Networks. *J. Sens.* **2016**, *2016*, 5725836. [[CrossRef](#)]
16. Shrestha, S.; Noh, S.K.; Choi, D.Y. Comparative study of antenna designs for RF energy harvesting. *Int. J. Antennas Propag.* **2013**, *2013*, 385260. [[CrossRef](#)]
17. Kraus, J.D.; Marhefka, R.J. *Antennas for All Applications*, 3rd ed.; McGraw-Hill: New York, NY, USA, 2002.
18. Garg, A.I.R.; Bhartia, P.; Bahl, I.J. *Microstrip Antenna Design Handbook*; Artech House: Norwood, MA, USA, 2001.
19. James, J.R.; Hall, P.S.; Wood, C. *Microstrip Antenna Theory and Design*; Peter Peregrinus Ltd.: London, UK, 1981.
20. Chandrasekaran, K.T.; Nasimuddin, N.; Alphonse, A.; Karim, M.F. Compact circularly polarized beam-switching wireless power transfer system for ambient energy harvesting applications. *Int. J. RF Microw. Comput. Eng.* **2019**, *29*, e21642. [[CrossRef](#)]
21. Hu, Y.Y.; Sun, S.; Xu, H. Compact Collinear Quasi-Yagi Antenna Array for Wireless Energy Harvesting. *IEEE Access.* **2020**, *8*, 35308–35317. [[CrossRef](#)]
22. Collado, A.; Member, S.; Georgiadis, A. A Compact Dual-Band Rectenna Using Slot-Loaded. *IEEE Antennas Wirel. Propag. Lett.* **2013**, *12*, 1634–1637.
23. Huang, F.J.; Yo, T.C.; Lee, C.M.; Luo, C.H. Design of circular polarization antenna with harmonic suppression for rectenna application. *IEEE Antennas Wirel. Propag. Lett.* **2012**, *11*, 592–595. [[CrossRef](#)]
24. Song, C.; Huang, Y.; Zhou, J.; Zhang, J.; Yuan, S.; Carter, P. A high-efficiency broadband rectenna for ambient wireless energy harvesting. *IEEE Trans. Antennas Propag.* **2015**, *63*, 3486–3495. [[CrossRef](#)]
25. Sun, H.; Guo, Y.X.; He, M.; Zhong, Z. Design of a high-efficiency 2.45-GHz rectenna for low-input-power energy harvesting. *IEEE Antennas Wirel. Propag. Lett.* **2012**, *11*, 929–932.
26. Lin, W.; Ziolkowski, R.W. Electrically Small, Single-Substrate Huygens Dipole Rectenna for Ultra-Compact Wireless Power Transfer Applications. *IEEE Trans. Antennas Propag.* **2020**, *69*, 1130–1134. [[CrossRef](#)]

27. Wang, M.S.; Zhu, X.Q.; Guo, Y.X.; Wu, W. Compact Circularly Polarized Patch Antenna with Wide Axial-Ratio Beamwidth. *IEEE Antennas Wirel. Propag. Lett.* **2018**, *17*, 714–718. [[CrossRef](#)]
28. Das, T.K.; Dwivedy, B.; Behera, D.; Behera, S.K.; Karmakar, N.C. Design and modelling of a compact circularly polarized antenna for RFID applications. *AEU-Int. J. Electron. Commun.* **2020**, *123*, 153313. [[CrossRef](#)]
29. Chandrasekaran, K.T.; Agarwal, K.; Nasimuddin; Alphones, A.; Mitra, R.; Karim, M.F. Compact Dual-Band Metamaterial-Based High-Efficiency Rectenna: An Application for Ambient Electromagnetic Energy Harvesting. *IEEE Antennas Propag. Mag.* **2020**, *62*, 18–29. [[CrossRef](#)]
30. Rosenblatt, G.; Orenstein, M. Perfect lensing with lossy metamaterials: Maintaining a singular focus by avoiding feedback. In Proceedings of the 2016 Progress in Electromagnetic Research Symposium (PIERS), Shanghai, China, 8–11 August 2016; p. 4946.
31. Upender, P.; Kumar, A. THz Dielectric Metamaterial Sensor With High Q for Biosensing Applications. *IEEE Sens. J.* **2023**, *23*, 5737–5744. [[CrossRef](#)]
32. Singh, H.; Mittal, N.; Gupta, A.; Kumar, Y.; Woźniak, M.; Waheed, A. Metamaterial integrated folded dipole antenna with low SAR for 4G, 5G and NB-IoT applications. *Electronics* **2021**, *10*, 2612. [[CrossRef](#)]
33. Sun, Z.; Zhao, X.; Zhang, L.; Mei, Z.; Zhong, H.; You, R.; Lu, W.; You, Z.; Zhao, J. WiFi energy-harvesting antenna inspired by the resonant magnetic dipole metamaterial. *Sensors* **2022**, *22*, 6523. [[CrossRef](#)] [[PubMed](#)]
34. Amer, A.A.G.; Othman, N.; Sapuan, S.Z.; Alphones, A.; Hassan, M.F.; Al-Gburi, A.J.A.; Zakaria, Z. Dual-Band, Wide-Angle, and High-Capture Efficiency Metasurface for Electromagnetic Energy Harvesting. *Nanomaterials* **2023**, *13*, 2015. [[CrossRef](#)]
35. Amer, A.A.G.; Sapuan, S.Z.; Ashyap, A.Y. Efficient metasurface for electromagnetic energy harvesting with high capture efficiency and a wide range of incident angles. *J. Electromagn. Waves Appl.* **2023**, *37*, 245–256. [[CrossRef](#)]
36. Packard, H. Technical Data, “Surface Mount Microwave Schottky Detector Diodes”. 1999. Available online: https://www.google.com.hk/url?sa=t&rct=j&q=&esrc=s&source=web&cd=&ved=2ahUKEwi3ueX52JCBAxWWiYBHxeQD6wQFnoECA4QAQ&url=http%3A%2F%2Fwww.hp.woodshot.com%2Fhpfrhelp%2F4_downld%2Fproducts%2Fdiodes%2Fhms2850.pdf&usq=AOvVaw3Q6hCE3Xm0w2WwkArNd2m_&opi=89978449 (accessed on 16 August 2023).
37. Song, C.; Huang, Y.; Carter, P.; Zhou, J.; Yuan, S.; Xu, Q.; Kod, M. A novel six-band dual CP rectenna using improved impedance matching technique for ambient RF energy harvesting. *IEEE Trans. Antennas Propag.* **2016**, *64*, 3160–3171. [[CrossRef](#)]
38. Geozondas.com. Time Domain Antenna Measurement Systems. [Online]. Available online: https://www.geozondas.com/main_page.php?pusl=12 (accessed on 20 July 2023).

Disclaimer/Publisher’s Note: The statements, opinions and data contained in all publications are solely those of the individual author(s) and contributor(s) and not of MDPI and/or the editor(s). MDPI and/or the editor(s) disclaim responsibility for any injury to people or property resulting from any ideas, methods, instructions or products referred to in the content.